Article

Cell Chemical Biology

Rescue of Pink1 Deficiency by Stress-Dependent Activation of Autophagy

Graphical Abstract

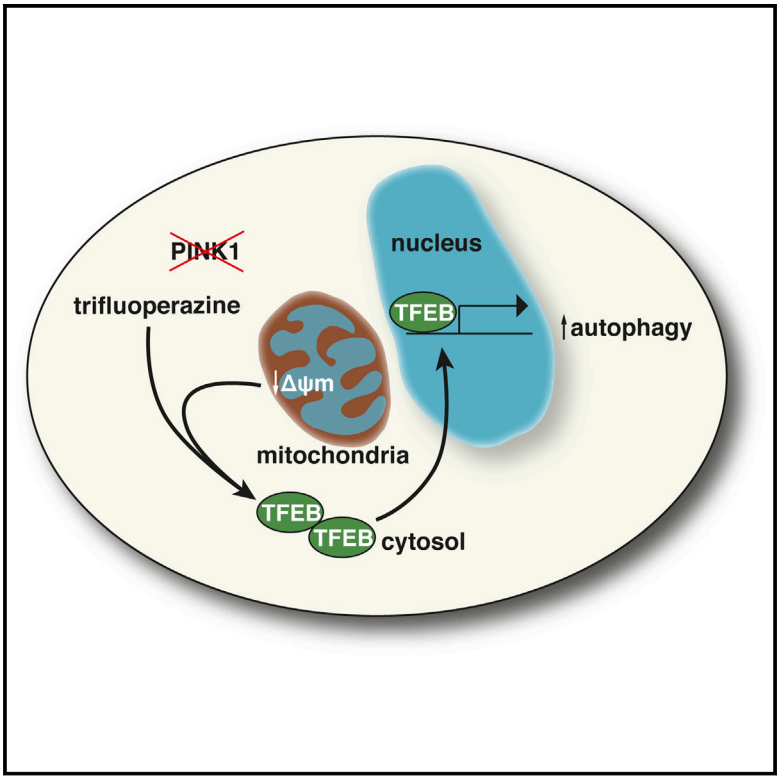

Authors

Yuxi Zhang, David T. Nguyen, Ellen M. Olzomer, ..., Anita Puvanendran, Brigitte R. Phillips, Daniel Hesselson

Correspondence

d.hesselson@garvan.org.au

In Brief

Zhang et al. established an in vivo phenotypic screen identifying autophagy-stimulating compounds that synergized with mitochondrial damage to rescue a zebrafish model of Parkinson's disease.

Highlights

- New zebrafish screening platform for Parkinson's disease
- Models mitochondrial dysfunction caused by genetic and environmental risk factors
- Identified trifluoperazine, which stimulates stress-dependent autophagy
- Trifluoperazine acts downstream of PINK1/PARKIN to restore TFEB nuclear translocation

Zhang et al., 2017, Cell Chemical Biology *24*, 1–10
April 20, 2017
http://dx.doi.org/10.1016/j.chembiol.2017.03.005

CellPress

Please cite this article in press as: Zhang et al., Rescue of Pink1 Deficiency by Stress-Dependent Activation of Autophagy, Cell Chemical Biology (2017), http://dx.doi.org/10.1016/j.chembiol.2017.03.005

Cell Chemical Biology
Article

Rescue of Pink1 Deficiency by Stress-Dependent Activation of Autophagy

Yuxi Zhang,[1] David T. Nguyen,[1] Ellen M. Olzomer,[1] Gin P. Poon,[1] Nicholas J. Cole,[2] Anita Puvanendran,[1] Brigitte R. Phillips,[1] and Daniel Hesselson[1,3,4,*]
[1]Diabetes and Metabolism Division, Garvan Institute of Medical Research, Sydney, NSW 2010, Australia
[2]Department of Biomedical Sciences, Faculty of Medicine and Health Sciences, Macquarie University, Sydney, NSW 2109, Australia
[3]St. Vincent's Clinical School, UNSW Australia, Sydney, NSW 2010, Australia
[4]Lead Contact
*Correspondence: d.hesselson@garvan.org.au
http://dx.doi.org/10.1016/j.chembiol.2017.03.005

SUMMARY

Stimulating autophagy is a promising therapeutic strategy for slowing the progression of neurodegenerative disease. Neurons are insensitive to current approaches based on mTOR inhibition for activating autophagy, and instead may rely on the Parkinson's disease-associated proteins PINK1 and PARKIN to activate the autophagy-lysosomal pathway in response to mitochondrial damage. We developed a multifactorial zebrafish drug-screening platform combining Pink1 deficiency with an environmental toxin to compromise mitochondrial function and trigger dopaminergic neuron loss. Using a phenotypic screening strategy, we identified a series of piperazine phenothiazines, including trifluoperazine, which rescued Pink1 deficiency by activating autophagy selectively in stressed zebrafish and human cells. We show that trifluoperazine acts downstream of, or parallel to, PINK1/PARKIN to stimulate transcription factor EB nuclear translocation and the expression of autophagy-lysosomal target genes. These data suggest that stress-dependent pharmacological reactivation of autophagy could prevent the loss of vulnerable neurons to slow neurodegeneration.

INTRODUCTION

Despite a growing consensus that the risk of Parkinson's disease (PD) is determined by a combination of genetic (Trinh and Farrer, 2013) and environmental (Tanner et al., 2011) factors, few studies have modeled their joint contributions to disease. PD-associated neuronal loss is associated with localized mitochondrial dysfunction before the clinical onset of motor symptoms (Hattingen et al., 2009). Existing treatments provide temporary symptomatic relief without restoring mitochondrial function or slowing disease progression (Schapira et al., 2014). It is clear that effective PD drug discovery will require improved high-throughput multifactorial models to identify disease-modifying interventions.

Defective mitochondria are a hallmark of neurodegenerative disease (Lin and Beal, 2006). Mitochondrial quality control has emerged as a potential therapeutic target based on the identification of *PINK1* (PTEN-induced kinase 1) and *PARK2* (PARKIN) mutations in autosomal-recessive PD pedigrees (Kitada et al., 1998; Valente et al., 2004). Mutations that impair PINK1 or PARKIN function cause the premature loss of dopaminergic (DA) neurons within the substantia nigra, which is associated with impaired autophagy of damaged mitochondria (mitophagy) (Pickrell and Youle, 2015). In addition to its role in mitophagy, PINK1 has also been associated with PARKIN-independent defects in mitochondrial oxidative phosphorylation (Morais et al., 2009). Reduced electron transport chain complex I activity (Parker and Swerdlow, 1998) and defective mitophagy (Hsieh et al., 2016) are also observed in models of sporadic PD, suggesting that these defects contribute to a common disease mechanism.

PINK1 function is evolutionarily conserved. *Drosophila* mutants lacking *pink1* exhibit muscle and DA neuron degeneration (Clark et al., 2006; Park et al., 2006; Yang et al., 2006) that can be rescued by the transgenic induction of autophagy (Liu and Lu, 2010). Surprisingly, Pink1-deficient mice exhibit subtle behavioral phenotypes without DA neuron loss (Kitada et al., 2007). However, DA neurons from Pink1-deficient mice are sensitized to the complex I toxin 1-methyl-4-phenyl-1,2,3,6-tetrahydropyridine (MPTP) and rescued by overexpression of the PD-associated genes *Parkin* or *DJ-1* (Haque et al., 2012). Thus, in addition to pharmacological stimulation of PINK1 kinase activity (Hertz et al., 2013), pathways acting downstream of, or parallel with, PINK1 provide additional therapeutic targets for PD.

Mitochondrial turnover is ultimately dependent on the degradative capacity of the autophagy-lysosomal pathway (ALP). Damaged mitochondria produce a signal that triggers nuclear translocation of the transcription factor EB (TFEB) (Ivankovic et al., 2015; Nezich et al., 2015), which induces lysosomal biogenesis (Sardiello et al., 2009) and upregulation of the core autophagy machinery (Settembre et al., 2011). While overexpression of TFEB is neuroprotective in murine PD models (Decressac et al., 2013), constitutive activation of the ALP is associated with oncogenesis (Kuiper et al., 2003), indicating that indiscriminate activation of TFEB must be avoided. TFEB translocation is stimulated by diverse signals (Roczniak-Ferguson et al., 2012; Settembre et al., 2012). Importantly, PINK1/PARKIN

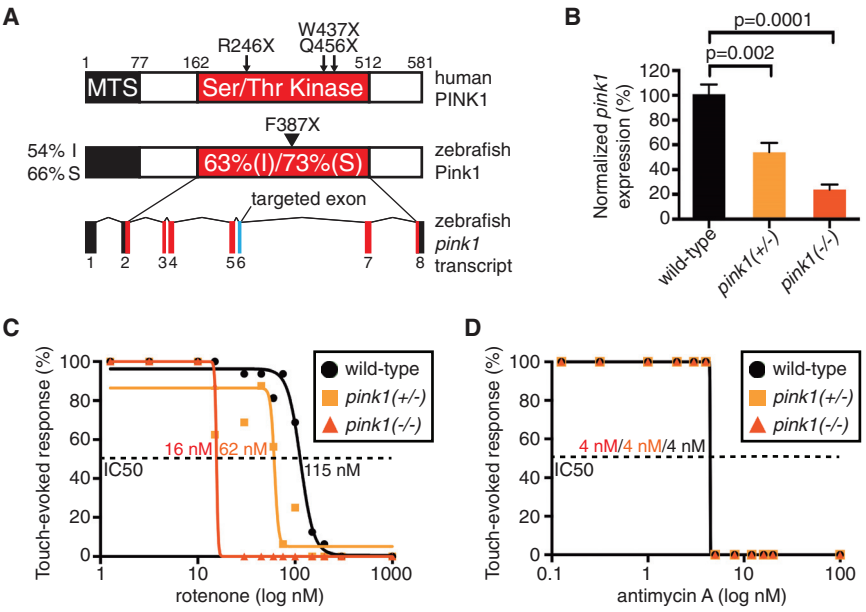

Figure 1. Zebrafish *pink1*$^{-/-}$ Mutants Are Sensitized to Complex I Inhibition

(A) Phylogenetic conservation of Pink1 protein structure and sequence (I, percent identity; S, percent similarity with human PINK1). Arrows indicate the positions of disease-associated premature stop codons in human PINK1. Arrowhead indicates the position of the TALEN-induced truncation (F387X) in *pink1*^{gi2} mutants.

(B) qRT-PCR analysis of *pink1* mRNA expression levels. Mean values ± SEM. n = 4 pools of ten zebrafish at 72 hr post fertilization (hpf) for each genotype. p Values determined by single-factor ANOVA with Dunnett's post hoc test.

(C and D) Dose-response curves for the effect of (C) complex I (rotenone) and (D) complex III (antimycin A) inhibition on the touch-evoked escape response. Treatment from 52 to 76 hpf. n = 16 zebrafish per genotype and dose. IC_{50} (half-maximal inhibitory concentration) determined by fitting a four-parameter sigmoidal curve to the data.

See also Figure S1.

are specifically required for TFEB nuclear translocation in response to mitochondrial stress (Nezich et al., 2015).

Using a high-throughput chemical genetic approach, we identified neuroprotective small molecules that rescued stress-induced mitochondrial dysfunction and prevented DA neuron loss in a zebrafish model of Pink1 deficiency. The most potent hit, the antipsychotic drug trifluoperazine (TFP), increased autophagic flux and restored stress-dependent activation of TFEB in PINK1-deficient human cells. Critically, we show that TFP acts synergistically with mitochondrial damage, suggesting that pharmacological reactivation of TFEB could prevent neurodegeneration without pathological induction of the ALP in non-neuronal tissues.

RESULTS

Pink1-Deficient Zebrafish are Sensitized to Complex I Inhibition

The majority of PD-associated PINK1 mutations cluster within the serine/threonine kinase domain (Song et al., 2013), including alleles that encode catalytically dead truncated PINK1 proteins (Figure 1A, arrows) (Hatano et al., 2004; Hedrich et al., 2006; Valente et al., 2004). PINK1 is highly conserved, with the kinase domain showing 63% identity and 73% similarity between human and zebrafish homologs. To generate a Pink1-deficient zebrafish model we disrupted the kinase domain using transcription activator-like effector nucleases (TALENs), which introduced a premature stop codon at position 387 (Figure 1A, arrowhead). Consistent with nonsense-mediated degradation of the mutant transcript, heterozygous *pink1*$^{+/gi2}$ and homozygous *pink1*$^{gi2/gi2}$ mutants (hereafter referred to as *pink1*$^{+/-}$ and *pink1*$^{-/-}$, respectively) had reduced levels of *pink1* mRNA (Figure 1B).

Similarly to Pink1-deficient mice (Kitada et al., 2007), zebrafish lacking *pink1* do not exhibit any obvious movement defects and both males and females are fertile (Flinn et al., 2013). We established a simple touch-evoked escape response (TEER) assay to test whether *pink1*$^{-/-}$ mutants are sensitized to pharmacological electron transport chain inhibition. Under basal conditions *pink1*$^{-/-}$ mutants and wild-type controls moved reproducibly in response to physical stimulation (n > 1,000). However, 24 hr of treatment with rotenone, a complex I inhibitor, disrupted the TEER in *pink1*$^{-/-}$ mutants at doses that did not impair wild-type controls (Figure 1C). The *pink1*$^{+/-}$ heterozygotes exhibited an intermediate sensitivity to rotenone (Figure 1C), indicating that maximal Pink1 activity is required under stressed conditions. The *pink1*$^{-/-}$ mutants also exhibited greater sensitivity to a structurally distinct complex I inhibitor, piericidin A (Figure S1). In contrast, *pink1* genotype did not affect sensitivity to the complex III inhibitor antimycin A (Figure 1D). Together, our data show that Pink1-deficient zebrafish are specifically sensitized to complex I inhibition.

To determine whether the sensitivity of *pink1*$^{-/-}$ mutants to rotenone was due to impaired mitochondrial function, we isolated mitochondria from zebrafish that were either grown under basal conditions or exposed to low-dose rotenone. Wild-type mitochondrial complex I activity (Figure S2A) and ATP content (Figure S2C) were unaffected by low-dose rotenone treatment. Despite exhibiting reduced complex I activity (Figure S2A) and membrane potential (Figures S2B and S2D), mitochondrial ATP content was maintained in *pink1*$^{-/-}$ mutants under basal conditions (Figure S2C). However, rotenone induced a synergistic loss of mitochondrial ATP content in *pink1*$^{-/-}$ mutants (interaction effect, p = 0.004; Figures S2A–S2C). Consistent with the data from the TEER assay, *pink1*$^{+/-}$ heterozygotes exhibited an intermediate mitochondrial phenotype (Figures S2A–S2C). To determine whether ex vivo mitochondrial activity is reflective of total respiratory capacity, we measured the oxygen consumption rate during a mitochondrial stress test using intact zebrafish (Figure 2A). Rotenone treatment or Pink-1 deficiency alone had no effect, whereas *pink1*$^{-/-}$ mutants treated with rotenone exhibited reduced basal and maximal oxygen consumption (interaction

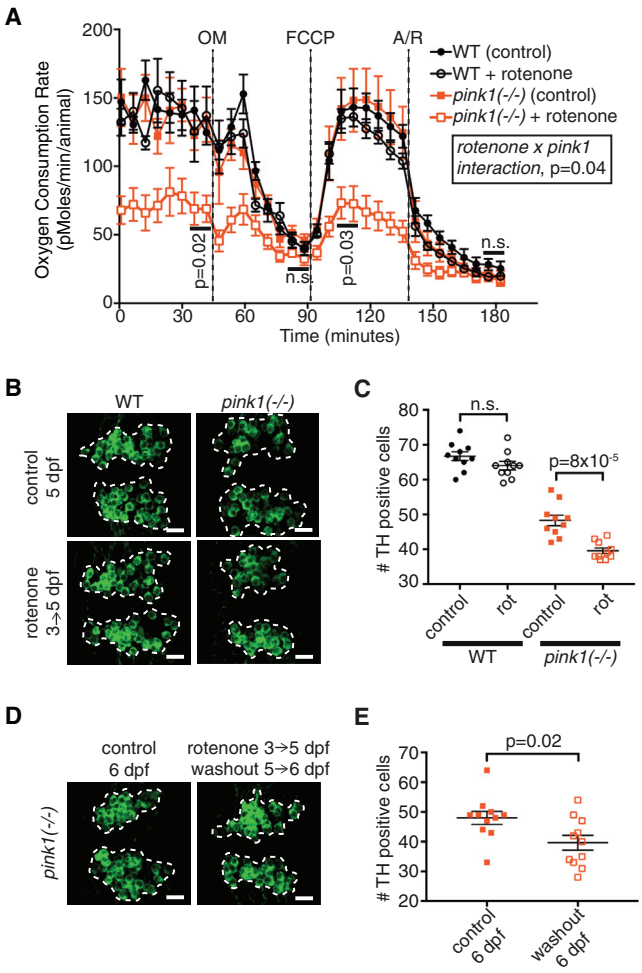

Figure 2. Mitochondrial Dysfunction and Neuronal Loss in a Zebrafish PD Model

(A) Oxygen consumption rate during an in vivo mitochondrial stress test. Zebrafish at 48 hpf were treated with rotenone (50 nM) or control culture medium for 6 hr. Oligomycin (OM), carbonyl cyanide 4-(trifluoromethoxy) phenylhydrazone (FCCP), and antimycin A + rotenone (A/R) were added consecutively. WT, wild-type. Mean values ± SEM. n = 5 animals per condition, representative of five independent experiments. Consecutive measurements were averaged as indicated and p values determined by two-way ANOVA with Tukey's post hoc test.

(B–E) Zebrafish were exposed to 5 nM rotenone or control conditions. (B and D) Confocal projections of DA neurons marked by anti-TH immunofluorescence. Dashed lines indicate regions selected for quantification. Scale bars represent 20 μm. (C and E) Quantification of TH^+ DA neurons in confocal reconstructions. (C) Mean values ± SEM. n = 10 samples per group. p Values determined by two-way ANOVA with Tukey's post hoc test. n.s., not significant. (E) Mean values ± SEM. n = 11 samples per group. p Values determined by two-tailed Student's t test.

See also Figure S2.

effect, p = 0.04; Figure 2A). These data indicate that Pink1 is required in vivo for the adaptive response to mitochondrial stress.

Although global mitochondrial respiration was unaffected in *pink1*$^{-/-}$ mutants under basal conditions (Figure 2A), DA neurons in the substantia nigra exhibit elevated sensitivity to mitochondrial dysfunction (Lin and Beal, 2006). The midbrain DA neuron populations 5, 6, and 11 (Kaslin and Panula, 2001; Rink and Wullimann, 2001) are also sensitive to the PD toxin MPTP in zebrafish (Sallinen et al., 2009), suggesting possible anatomical and functional conservation. These populations could be clearly distinguished by immunofluorescent tyrosine hydroxylase (TH) staining and exhibited a 30%–40% deficiency in *pink1*$^{-/-}$ mutants compared with controls (Figures S2E and S2F). We established an extended treatment protocol to test whether ultra-low-dose rotenone (5 nM) enhanced the loss of DA neurons in *pink1*$^{-/-}$ mutants. A 2-day exposure did not affect the number of DA neurons in wild-type animals but this mild mitochondrial stress was sufficient to further reduce the number of midbrain 5, 6, and 11 DA neurons in Pink1-deficient animals (interaction effect, p = 0.02; Figures 2B and 2C), without affecting the number of DA neurons in an adjacent brain region (Figures S2G and S2H). To determine whether the loss of TH staining was due to transient loss of TH expression in stressed neurons, we washed out the toxin and allowed the animals to recover for 1 day. Rotenone-treated *pink1*$^{-/-}$ mutants continued to exhibit a reduced number of TH^+ cells after the washout (Figures 2D and 2E), indicating that susceptible DA neurons did not rapidly redifferentiate or had been eliminated.

Unbiased Identification of Neuroprotective Small Molecules

We optimized a chemical genetic screen to identify small molecules that rescued the rotenone sensitivity of our PD model using the TEER assay. Rotenone treatment (45 nM) for 24 hr was sufficient to prevent touch-evoked movement in *pink1*$^{-/-}$ mutants (n > 1,000). Because the production of reactive oxygen species (ROS) is correlated with neurodegeneration (Lin and Beal, 2006), we first tested whether the screen would identify molecules with antioxidant activity. Rotenone-treated *pink1*$^{-/-}$ mutants exhibited elevated levels of ROS that were normalized by supplementation with the glutathione precursor *N*-acetylcysteine (Figure S3A). However, *N*-acetylcysteine treatment did not restore movement in the TEER assay (Figure S4A), indicating that ROS suppression is not sufficient for rescue.

We proceeded to screen the NIH Clinical Collection (Evotec, 727 compounds) (Figure 3A). Three structurally related piperazine phenothiazines were the only compounds that restored movement in the primary screen (Figure 3B). TFP, fluphenazine (FLU), and prochlorperazine (PRO) obtained from an independent vendor exhibited robust rescue activity in an orthogonal whole-embryo ATP assay (Figure 3C). We performed acute ex vivo mitochondrial treatments to determine whether screen hits interfered with rotenone-mediated complex I inhibition. Co-treatment of isolated mitochondria with TFP and rotenone did not block rotenone action (Figure S3B). In addition, TFP rescued in vivo ATP levels in *pink1*$^{-/-}$ mutants stressed with a structurally distinct complex I inhibitor (Figure S3C). Together, these data indicate that rescuing compounds act downstream of complex I inhibition.

The TFP/FLU/PRO pharmacophore has previously been implicated in the regulation of autophagy (Tsvetkov et al., 2010), although its mechanism of action remains unclear. We next tested whether rescue was associated with increased

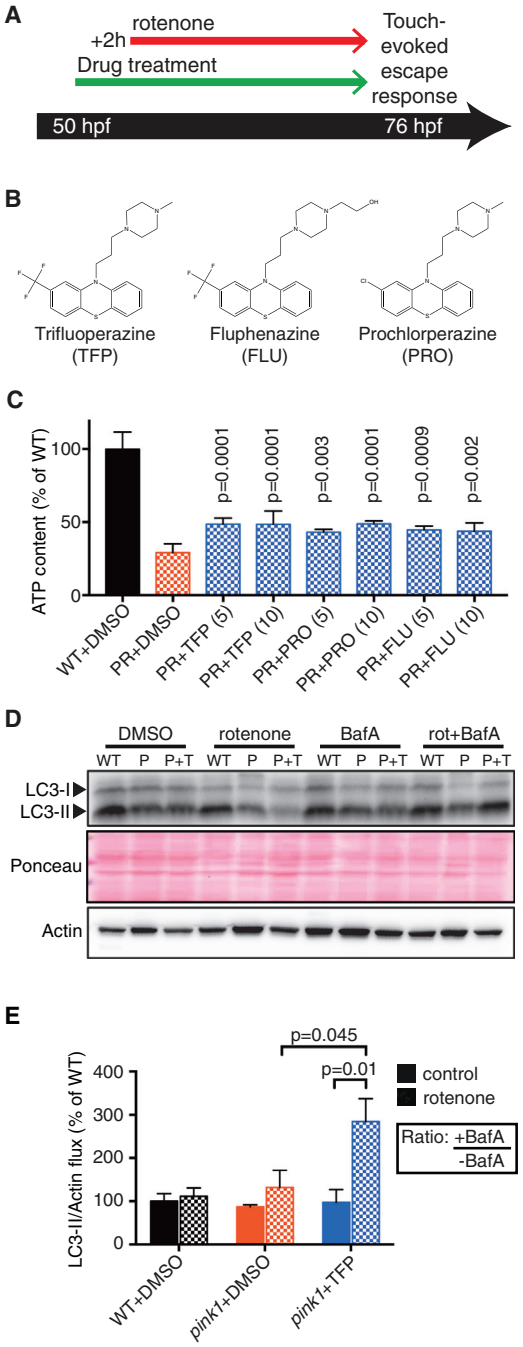

Figure 3. Chemical Genetic Screen for Phenotypic Rescue of a Zebrafish PD Model

(A) Touch-evoked escape response screen. The NIH Clinical Collection was screened in 96-well plates. Two *pink1*$^{-/-}$ mutants were incubated with 10 μM of each compound for 2 hr followed by 24 hr of exposure to 45 nM rotenone (1% final DMSO concentration).

(B) Three structurally related piperazine phenothiazines exhibited rescue.

(C) Whole-animal ATP content was quantified in zebrafish that were treated with small molecules from 48 to 50 hpf at 5 or 10 μM (1% final DMSO concentration) followed by exposure to 80 nM rotenone for 4 hr. WT, wild-type; PR, *pink1*$^{-/-}$ + rotenone. Mean values ± SEM. n = 4 pools of six animals for each genotype and condition. p Values for rescue determined by single-factor ANOVA with Dunnett's post hoc test.

(D and E) Pools of 50 zebrafish (48 hpf) were pretreated with 8 μM TFP or 1% DMSO for 2 hr and then exposed to rotenone (80 nM) ± BafA (10 nM) as indicated for 4 hr. (D) LC3-I and LC3-II protein levels in wild-type (WT), *pink1*$^{-/-}$ (P), and *pink1*$^{-/-}$ + TFP (P+T). Actin levels and Ponceau staining were used as loading controls. (E) Quantification of LC3-II flux. The ratio of actin-normalized LC3-II levels with and without BafA treatment was determined for three independent biological samples. Mean values ± SEM. p Values determined by two-way ANOVA with Tukey's post hoc test.

See also Figures S3 and S4.

autophagic flux. To this end we measured the levels of the core autophagosome component LC3-II in the presence or absence of the autolysosomal inhibitor bafilomycin A (BafA) at a dose that blocks lysosomal activity without impairing mitochondrial function (Figures S3D–S3F). Whereas steady-state LC3-II levels are determined by the relative rates of autophagy initiation and completion, the extent of LC3-II accumulation in BafA-treated animals corresponds to flux through the autophagic pathway (Klionsky et al., 2016). TFP only stimulated autophagic flux in rotenone-stressed *pink1*$^{-/-}$ mutants (Figures 3D and 3E), indicating that autophagic stimulation requires a stress-induced co-stimulatory signal in vivo.

To determine whether pharmacological rescue required a functional autophagic pathway, we analyzed mitochondria isolated from rotenone-stressed *pink1*$^{-/-}$ mutants. TFP treatment increased complex I activity (Figure S4C), membrane potential (Figure S4D), and ATP content (Figure S4E), and the protective effect was inhibited by co-treatment with BafA (Figures S4C–S4E). Consistent with its protective effects on isolated mitochondria, TFP increased basal and maximal oxygen consumption in vivo (Figures 4A and S4B). The stimulatory effect of TFP on maximal oxygen consumption was blunted by co-treatment with BafA (Figures 4A and S4B), further supporting a role for autophagy in its protective mechanism. Next, we explored whether improved mitochondrial function in TFP-treated animals translated to protection of vulnerable neurons. Treatment with TFP prevented rotenone-induced neuron loss in Pink1-deficient animals (Figures 4B and 4C) and this effect was blocked by co-treatment with BafA (Figures 4D and 4E). Finally, using the TEER assay we determined that BafA treatment (Figure 4F) or knockdown of the core autophagy component *atg5* (Varga et al., 2014) (Figure 4G) blocked TFP-mediated rescue. We conclude that TFP requires a functional autophagic pathway to restore mitochondrial function and induce phenotypic rescue of the zebrafish PD model.

Stress-Dependent TFEB Activation

Depolarized mitochondria generate a PINK1/PARKIN-dependent signal that stimulates nuclear translocation of TFEB to activate autophagic target genes including *SQSTM1* (also known as *p62*) (Ivankovic et al., 2015; Nezich et al., 2015). We used lentiviral knockdown in human SH-SY5Y neuroblastoma cells (Figure S5D) to determine whether TFP treatment restored the cellular response to mitochondrial damage downstream of PINK1 and/or PARKIN. In short-hairpin control (shControl) cells, TFP treatment or mitochondrial stress induced by oligomycin/antimycin A did not alter *SQSTM1* mRNA levels, whereas combinatorial treatment synergistically activated *SQSTM1* transcription (interaction effect, p = 0.0003; Figure 5A). The

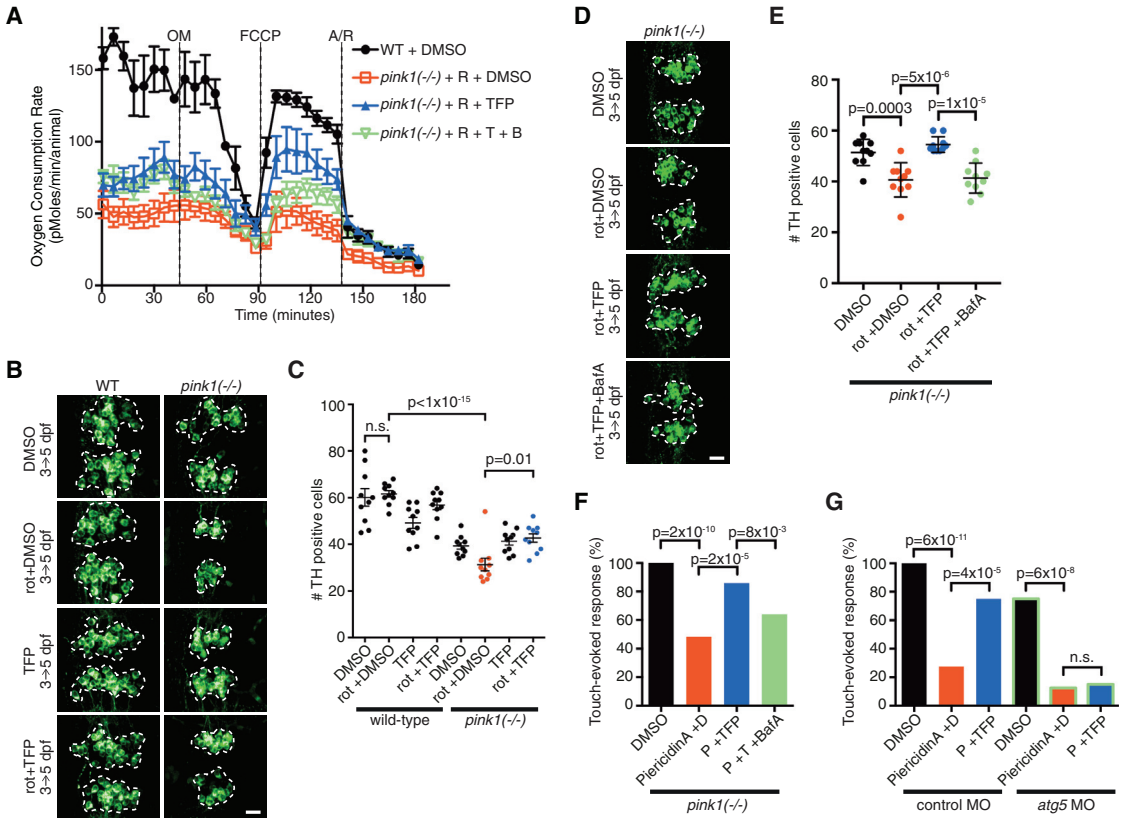

Figure 4. TFP Action Requires Autophagy to Restore Mitochondrial Function and Prevent DA Neuron Loss

(A) Oxygen consumption rate during an in vivo mitochondrial stress test. Zebrafish at 48 hpf were treated with R (80 nM rotenone), T (8 μM TFP), B (10 nM BafA), or control medium for 6 hr. Oligomycin (OM), FCCP, and antimycin A + rotenone (A/R) were added consecutively. Mean values ± SEM. n = 5 animals per condition, representative of four independent experiments.

(B–E) Zebrafish were treated with 5 μM TFP or 1% DMSO and exposed to 5 nM rotenone, 10 nM BafA, or control conditions for 2 days. (B and D) Confocal projections of DA neurons marked by anti-TH immunofluorescence. Dashed line indicates region selected for quantification. Scale bars represent 20 μm. (C and E) Quantification of TH^+ DA neurons in confocal reconstructions. Mean values ± SEM. n = 10 samples per group. p Values for treatment effects determined by (C) two-way ANOVA with Tukey's post hoc test or (E) single-factor ANOVA with Dunnett's post hoc test. n.s., not significant.

(F and G) Touch-evoked escape response in zebrafish at 72 hpf. (F) Zebrafish were treated with 8 μM TFP (±20 nM BafA) or DMSO for 2 hr followed by 24 hr of exposure to 60 nM piericidin A. n = 64 zebrafish per group. p Values determined by chi-square with post hoc Benjamini-Yekutieli correction. (G) Control or *atg5* morpholino-injected zebrafish were treated with 5 μM TFP or DMSO for 2 hr followed by 24 hr of exposure to 80 nM piericidin A. n = 40 zebrafish per group. p Values determined by chi-square with post hoc Benjamini-Yekutieli correction.

See also Figures S3 and S4.

magnitude of the TFP-induced *SQSTM1* transcriptional response was enhanced in shPINK1 knockdown cells (interaction effect, $p = 5 \times 10^{-6}$; Figures 5A and 5B) and extended to additional TFEB target genes (Figures S5A–S5C). SQSTM1 recruits polyubiquitinated substrates to autophagosomes where it is degraded along with its cargo (Pankiv et al., 2007). TFP treatment increased SQSTM1 flux in stressed shPINK1 cells (interaction effect, $p = 3 \times 10^{-5}$; Figures 5B and 5C). TFP also increased LC3-II flux (Figures 5B and S5E), indicating that it exerts a global stimulatory effect on autophagy. Consistent with the slow mitophagy kinetics reported in SH-SY5Y cells that do not overexpress PARKIN (Geisler et al., 2010), mitochondrial MTCO2 flux was unaffected (Figures 5B and S5F). Together, our data indicate that TFP treatment also stimulated autophagy in stressed human cells.

To further define the mechanism of action for TFP, we analyzed the cellular events downstream of PINK1. PARKIN translocates from the cytoplasm to damaged mitochondria in a PINK1-dependent manner (Figures 6A and 6B) (Pickrell and Youle, 2015). TFP did not restore YFP-PARKIN translocation to mitochondria in stressed shPINK1 cells (Figures 6A and 6B), indicating that it acts downstream of, or parallel to, PARKIN. Next, we analyzed nuclear translocation of the downstream transcription factor TFEB. In shControl cells, mitochondrial damage induced nuclear EGFP-TFEB translocation, whereas TFP had no effect (Figures 7A and 7B). As reported (Ivankovic et al., 2015; Nezich et al., 2015), TFEB translocation was completely blocked in stressed shPINK1 cells, however, TFP treatment bypassed PINK1 to significantly increase TFEB nuclear translocation under these conditions (Figures 7A and 7B). To determine whether TFP analogs also regulated TFEB localization we tested PRO, FLU, and 10-[4′-(*N*-diethylamino)butyl]-2-chlorophenoxazine (10-NCP) (Tsvetkov et al., 2010) in the TFEB translocation assay. All three analogs induced TFEB nuclear translocation in stressed

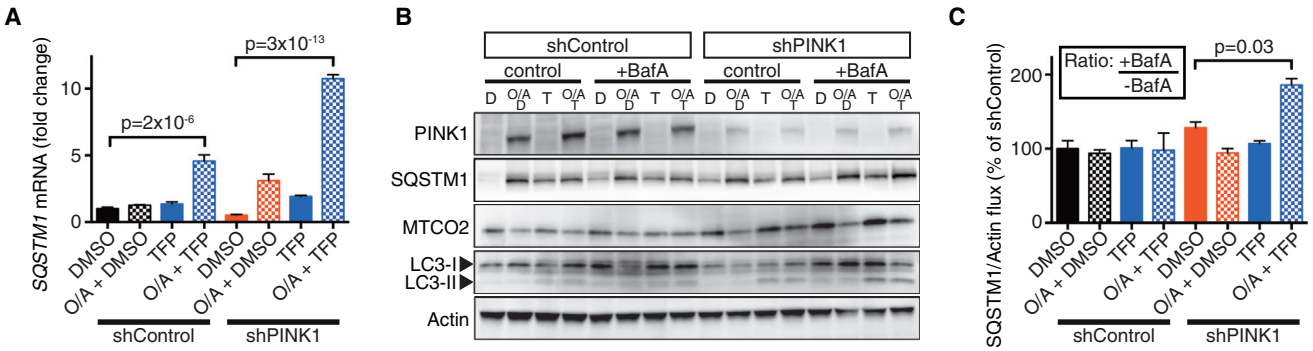

Figure 5. TFP Activates Stress-Dependent Autophagy

Human SH-SY5Y neuroblastoma cells were transduced with shPINK1 or shControl lentivirus. D, DMSO control; O/A, 10 μg/mL oligomycin A + 5 μg/mL antimycin A; T/TFP, 10 μM TFP.

(A) qRT-PCR analysis of *sqstm1* mRNA expression levels in cells that were treated for 24 hr as indicated. Mean values ± SEM. n = 3 biological replicates for each condition. p Values determined by two-way ANOVA with Tukey's post hoc test.

(B) PINK1, SQSTM1, MTCO2, LC3-I, and LC3-II protein levels in cells treated for 24 hr as indicated. BafA (100 nM) or vehicle control was added during the final hour of treatment. Actin was used as a loading control.

(C) The ratio of actin-normalized SQSTM1 levels with and without BafA treatment was determined for three independent biological samples. Mean values ± SEM. p values determined by two-way ANOVA with Tukey's post hoc test.

See also Figure S5.

shPINK1 cells (Figures S6C and S6D) although they also exhibited partial activity in unstressed control cells (Figures S6A and S6B). Similarly, mammalian target of rapamycin (mTOR) inhibition and β-cyclodextrin treatment (Song et al., 2014) stimulated TFEB nuclear translocation in unstressed control cells (Figures S6E and S6F). TFP also synergized with mitochondrial damage to induce *sqstm1* mRNA in vivo (interaction effect, p = 0.0006; Figure 7C), whereas the TFP analogs (PRO, FLU, and 10-NCP) lacked this activity (Figure S7). We conclude that TFP stimulates autophagic flux in cells with damaged mitochondria through PINK1-independent activation of the ALP.

DISCUSSION

High-throughput in vivo modeling of neurodegenerative disease for preclinical drug development is a major advance that can rapidly pinpoint new compounds for consideration in a PD drug development pipeline (Schapira et al., 2014). Because high-throughput screening in rodents or larger animals is generally not feasible, alternative systems including patient-derived stem cell models (Cooper et al., 2012; Khurana et al., 2015) have been developed for testing therapeutic agents; however, there is currently no adequate in vivo platform. Here we report a complementary vertebrate model that combines Pink1 deficiency with complex I inhibition to induce global mitochondrial dysfunction and specific loss of midbrain DA neurons. Importantly, our model mirrors the PD-specific sensitivity to complex I inhibition observed in patient-derived cells (Murtaza et al., 2016).

Nutritional or pharmacological inhibition of mTOR activates the ALP by stimulating nuclear translocation of TFEB (Roczniak-Ferguson et al., 2012; Settembre et al., 2012). However, differential regulation of neuronal and non-neuronal autophagy (Yue et al., 2009) suggests that mTOR inhibition will not be sufficient to restore autophagic flux in neurodegenerative disease. The carrier molecule 2-hydroxypropyl-β-cyclodextrin also activates TFEB (Song et al., 2014) to enhance the clearance of toxic aggregates in cells (Kilpatrick et al., 2015), although it requires millimolar dosing, potentially limiting its utility. Using an unbiased whole-organism phenotypic screen we identified TFP, a piperazine phenothiazine that has been shown to stimulate autophagy in cellular models of neurodegeneration (Hollerhage et al., 2014; Tsvetkov et al., 2010). However, its mechanism of action and in vivo activity has not been explored. We show that TFP acts downstream of, or parallel to, PARKIN to restore TFEB nuclear localization and increase autophagic flux specifically in cells and animals with impaired mitochondrial function. TFP showed partial activity in shPINK1 cells under basal conditions. Similar PINK1 knockdown models exhibited impaired mitochondrial function (Wood-Kaczmar et al., 2008) and reduced expression of ALP proteins (Parganlija et al., 2014), suggesting that standard culture conditions generate an attenuated mitochondrial stress signal. It is not yet clear how mitochondrial damage contributes to TFEB activation, although the differential activity of TFP and its analogs in the TFEB translocation assay indicate that the combination of a specific tertiary amine and fluorinated phenothiazine residue are important for restricting activity to stressed cells. PINK1 also has autophagy-independent functions, including regulation of mitochondrial calcium homeostasis (Gandhi et al., 2009) and maintenance of complex I activity (Vilain et al., 2012). TFP rescue activity was only partially blocked by inhibiting autophagy, indicating that inhibition of additional targets (e.g., calmodulin [Vandonselaar et al., 1994]) may contribute to its protective mechanism, highlighting the power of phenotypic screens to simultaneously select for activity at multiple targets (MacRae and Peterson, 2015).

TFP is currently used as an antipsychotic to modulate dopamine receptor signaling in schizophrenia (Creese et al., 1976). The robust and sensitive in vivo bioassays presented here will

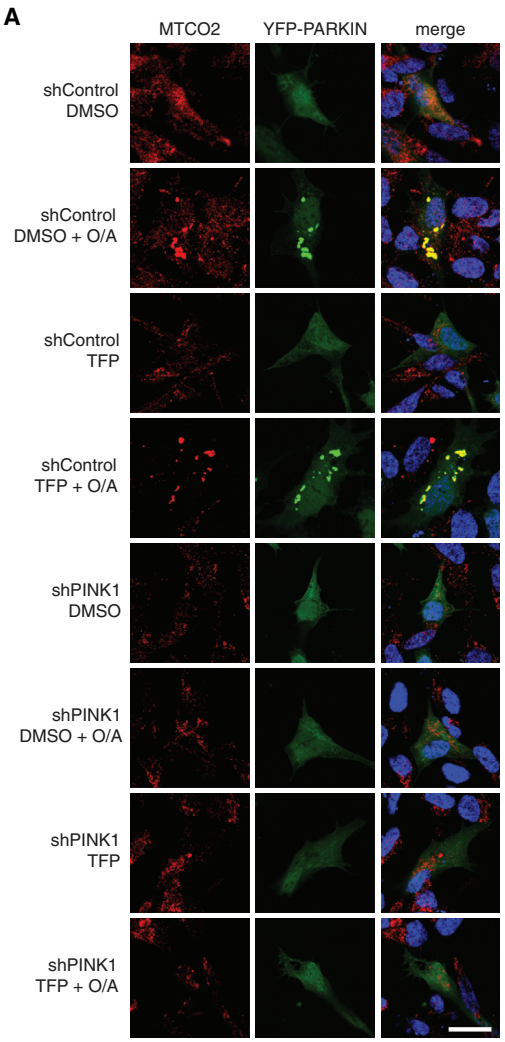

Figure 6. TFP Does Not Restore PARKIN Translocation to Damaged Mitochondria

Human SH-SY5Y neuroblastoma cells were transduced with shControl or shPINK1 lentivirus and transfected with a YFP-PARKIN expression construct. Cells were treated for 6 hr as indicated. O/A, 10 μg/mL oligomycin A + 5 μg/mL antimycin A; TFP, 10 μM trifluoperazine.

(A) Individual channels show mitochondrial MTCO2 immunofluorescence and YFP-PARKIN expression. Nuclei are marked with DAPI in the merged images. Scale bar represents 20 μm.

(B) Co-localization of MTCO2 with YFP-PARKIN in transfected cells was quantified using Coloc2 (ImageJ). The thresholded Pearson correlation (−1.0 to 1.0) for 30 cells is presented as mean values ± SEM. p Values determined by two-way ANOVA with Tukey's post hoc test. n.s., not significant.

aid the development of new clinical candidates for PD based on the TFP pharmacophore, which will require elimination of the antidopaminergic activity while maintaining selectivity for cells with mitochondrial damage to prevent off-target oncogenic activation of the ALP.

SIGNIFICANCE

Human genetics and epidemiology have identified Parkinson's disease (PD) risk factors that converge on pathways involved in mitochondrial function. However, it has been challenging to effectively model neurodegenerative disease in cell-based systems and screening strategies because rescue of age-associated neurodegenerative disease is generally not feasible in rodents or larger animals. In this work, we present an in vivo zebrafish screening platform that combines genetic and environmental risk factors, which synergize to produce mitochondrial dysfunction and dopaminergic neuron loss. While previous screens have identified small molecules that suppress genetic defects or the toxicity of environmental pollutants, this is the first report of a multifactorial vertebrate screening model for a complex disease. Using our novel zebrafish screening platform and mechanistic analyses in human cells, we identified three structurally related piperazine phenothiazines that induced phenotypic rescue in an autophagy-dependent manner. A potential downside of autophagy stimulation is that constitutive upregulation is linked to oncogenic outcomes. We show that the most potent hit (trifluoperazine) increased autophagy specifically in stressed zebrafish and human cells. Trifluoperazine acted downstream of, or parallel to, PINK1/PARKIN to restore TFEB translocation, which is a master regulator of the autophagy-lysosomal pathway. Our findings provide compelling rationale and robust bioassays for the development of a new class of stress-dependent autophagy-stimulating drugs for neurodegenerative disease.

STAR★METHODS

Detailed methods are provided in the online version of this paper and include the following:

- KEY RESOURCES TABLE
- CONTACT FOR REAGENT AND RESOURCE SHARING
- EXPERIMENTAL MODEL AND SUBJECT DETAILS
  - Zebrafish
  - Cell Lines
- METHODS DETAIL
  - TALEN Mutagenesis
  - Touch-Evoked Escape Response
  - Chemical Screen
  - Mitochondrial Isolation
  - Complex I Activity
  - Mitochondrial Membrane Potential

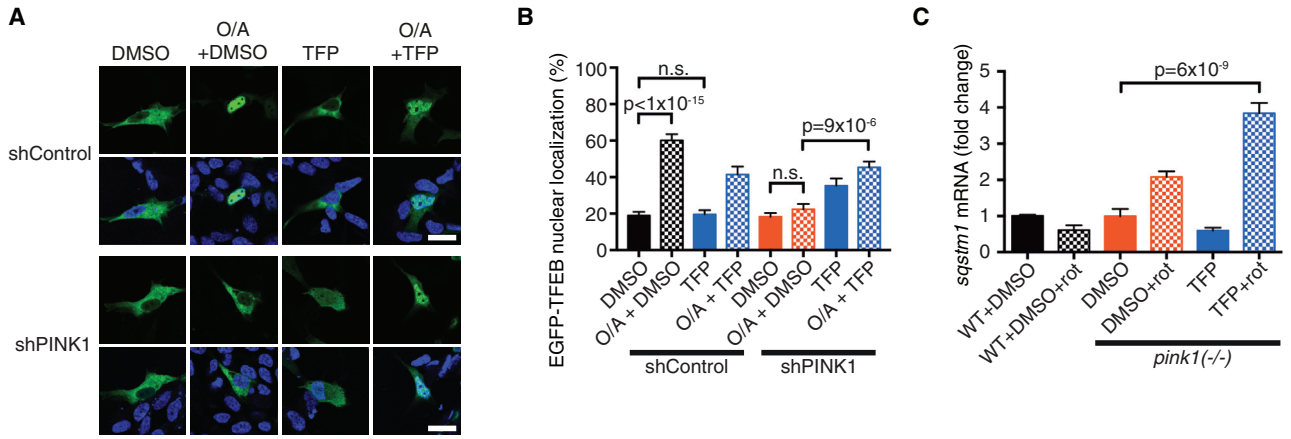

Figure 7. Pink1-Independent Rescue of TFEB Nuclear Translocation

(A and B) Human SH-SY5Y neuroblastoma cells were transduced with shPINK1 or shControl lentivirus. D, DMSO control; O/A, 10 μg/mL oligomycin A + 5 μg/mL antimycin A; T/TFP, 10 μM TFP. (A) Confocal sections of shPINK1 and shControl cells transfected with an EGFP-TFEB expression construct and treated for 6 hr as indicated. Nuclei are marked with DAPI. Scale bars represent 20 μm. (B) Quantification of EGFP-TFEB nuclear localization. Mean values ± SEM. n = 30 cells per condition. p Values determined by two-way ANOVA with Tukey's post hoc test. n.s., not significant.

(C) qRT-PCR analysis of zebrafish *sqstm1* mRNA expression levels. Zebrafish (48 hpf) were treated with TFP or 1% DMSO for 2 hr followed by exposure to rotenone (80 nM) or control culture media for 4 hr. Mean values ± SEM. n = 3 pools of 10 zebrafish for each genotype and treatment. p Values determined by two-way ANOVA with Tukey's post hoc test.

See also Figures S6 and S7.

- ATP Content
- ROS Production
- Mitochondrial Stress Test
- Tissue Culture and Drug Treatments
- Lentiviral PINK1 Knockdown
- Quantitative Real-Time PCR
- Immunostaining and Confocal Microscopy
- Western Blotting

● QUANTIFICATION AND STATISTICAL ANALYSIS

SUPPLEMENTAL INFORMATION

Supplemental Information includes seven figures and can be found with this article online at http://dx.doi.org/10.1016/j.chembiol.2017.03.005.

AUTHOR CONTRIBUTIONS

Conceptualization, D.H.; Methodology, Y.Z., D.T.N., E.M.O., A.P., and B.R.P.; Investigation, Y.Z., D.T.N., E.M.O., and G.P.P.; Resources, N.J.C.; Formal Analysis, D.H.; Visualization, D.H.; Writing – Original Draft, Y.Z. and D.H.; Writing – Review & Editing, Y.Z. and D.H.; Funding Acquisition, D.H.

ACKNOWLEDGMENTS

The authors thank G. Neely, K. Kikuchi, T. Biden, and S. Hesselson for critical reading of the manuscript; and J. Brand, M. Pickering, and L. Nedved for zebrafish care. This study was supported by an Australian NH&MRC grant GNT1063981 and Garvan Research Foundation grants to D.H.

Received: October 1, 2016
Revised: January 2, 2017
Accepted: March 2, 2017
Published: March 30, 2017

REFERENCES

Cermak, T., Doyle, E.L., Christian, M., Wang, L., Zhang, Y., Schmidt, C., Baller, J.A., Somia, N.V., Bogdanove, A.J., and Voytas, D.F. (2011). Efficient design and assembly of custom TALEN and other TAL effector-based constructs for DNA targeting. Nucleic Acids Res. *39*, e82.

Clark, I.E., Dodson, M.W., Jiang, C., Cao, J.H., Huh, J.R., Seol, J.H., Yoo, S.J., Hay, B.A., and Guo, M. (2006). *Drosophila* pink1 is required for mitochondrial function and interacts genetically with parkin. Nature *441*, 1162–1166.

Cooper, O., Seo, H., Andrabi, S., Guardia-Laguarta, C., Graziotto, J., Sundberg, M., McLean, J.R., Carrillo-Reid, L., Xie, Z., Osborn, T., et al. (2012). Pharmacological rescue of mitochondrial deficits in iPSC-derived neural cells from patients with familial Parkinson's disease. Sci. Transl. Med. *4*, 141ra190.

Creese, I., Burt, D.R., and Snyder, S.H. (1976). Dopamine receptor binding predicts clinical and pharmacological potencies of antischizophrenic drugs. Science *192*, 481–483.

Decressac, M., Mattsson, B., Weikop, P., Lundblad, M., Jakobsson, J., and Bjorklund, A. (2013). TFEB-mediated autophagy rescues midbrain dopamine neurons from alpha-synuclein toxicity. Proc. Natl. Acad. Sci. USA *110*, E1817–E1826.

Flinn, L.J., Keatinge, M., Bretaud, S., Mortiboys, H., Matsui, H., De Felice, E., Woodroof, H.I., Brown, L., McTighe, A., Soellner, R., et al. (2013). TigarB causes mitochondrial dysfunction and neuronal loss in PINK1 deficiency. Ann. Neurol. *74*, 837–847.

Gandhi, S., Wood-Kaczmar, A., Yao, Z., Plun-Favreau, H., Deas, E., Klupsch, K., Downward, J., Latchman, D.S., Tabrizi, S.J., Wood, N.W., et al. (2009). PINK1-associated Parkinson's disease is caused by neuronal vulnerability to calcium-induced cell death. Mol. Cell *33*, 627–638.

Geisler, S., Holmstrom, K.M., Skujat, D., Fiesel, F.C., Rothfuss, O.C., Kahle, P.J., and Springer, W. (2010). PINK1/Parkin-mediated mitophagy is dependent on VDAC1 and p62/SQSTM1. Nat. Cell Biol. *12*, 119–131.

Gibert, Y., McGee, S.L., and Ward, A.C. (2013). Metabolic profile analysis of zebrafish embryos. J. Vis. Exp. e4300.

Haque, M.E., Mount, M.P., Safarpour, F., Abdel-Messih, E., Callaghan, S., Mazerolle, C., Kitada, T., Slack, R.S., Wallace, V., Shen, J., et al. (2012). Inactivation of Pink1 gene in vivo sensitizes dopamine-producing neurons to 1-methyl-4-phenyl-1,2,3,6-tetrahydropyridine (MPTP) and can be rescued by autosomal recessive Parkinson disease genes, Parkin or DJ-1. J. Biol. Chem. *287*, 23162–23170.

Hatano, Y., Li, Y., Sato, K., Asakawa, S., Yamamura, Y., Tomiyama, H., Yoshino, H., Asahina, M., Kobayashi, S., Hassin-Baer, S., et al. (2004). Novel PINK1 mutations in early-onset parkinsonism. Ann. Neurol. *56*, 424–427.

Hattingen, E., Magerkurth, J., Pilatus, U., Mozer, A., Seifried, C., Steinmetz, H., Zanella, F., and Hilker, R. (2009). Phosphorus and proton magnetic resonance spectroscopy demonstrates mitochondrial dysfunction in early and advanced Parkinson's disease. Brain *132*, 3285–3297.

Hedrich, K., Hagenah, J., Djarmati, A., Hiller, A., Lohnau, T., Lasek, K., Grunewald, A., Hilker, R., Steinlechner, S., Boston, H., et al. (2006). Clinical spectrum of homozygous and heterozygous PINK1 mutations in a large German family with Parkinson disease: role of a single hit? Arch. Neurol. *63*, 833–838.

Hertz, N.T., Berthet, A., Sos, M.L., Thorn, K.S., Burlingame, A.L., Nakamura, K., and Shokat, K.M. (2013). A neo-substrate that amplifies catalytic activity of parkinson's-disease-related kinase PINK1. Cell *154*, 737–747.

Hollerhage, M., Goebel, J.N., de Andrade, A., Hildebrandt, T., Dolga, A., Culmsee, C., Oertel, W.H., Hengerer, B., and Hoglinger, G.U. (2014). Trifluoperazine rescues human dopaminergic cells from wild-type alpha-synuclein-induced toxicity. Neurobiol. Aging *35*, 1700–1711.

Hsieh, C.H., Shaltouki, A., Gonzalez, A.E., Bettencourt da Cruz, A., Burbulla, L.F., St Lawrence, E., Schule, B., Krainc, D., Palmer, T.D., and Wang, X. (2016). Functional impairment in miro degradation and mitophagy is a shared feature in familial and sporadic Parkinson's disease. Cell Stem Cell *19*, 709–724.

Ivankovic, D., Chau, K.Y., Schapira, A.H., and Gegg, M.E. (2015). Mitochondrial and lysosomal biogenesis are activated following PINK1/parkin-mediated mitophagy. J. Neurochem. *136*, 388–402.

Janssen, A.J., Trijbels, F.J., Sengers, R.C., Smeitink, J.A., van den Heuvel, L.P., Wintjes, L.T., Stoltenborg-Hogenkamp, B.J., and Rodenburg, R.J. (2007). Spectrophotometric assay for complex I of the respiratory chain in tissue samples and cultured fibroblasts. Clin. Chem. *53*, 729–734.

Kaslin, J., and Panula, P. (2001). Comparative anatomy of the histaminergic and other aminergic systems in zebrafish (*Danio rerio*). J. Comp. Neurol. *440*, 342–377.

Khurana, V., Tardiff, D.F., Chung, C.Y., and Lindquist, S. (2015). Toward stem cell-based phenotypic screens for neurodegenerative diseases. Nat. Rev. Neurol. *11*, 339–350.

Kilpatrick, K., Zeng, Y., Hancock, T., and Segatori, L. (2015). Genetic and chemical activation of TFEB mediates clearance of aggregated alpha-synuclein. PLoS One *10*, e0120819.

Kitada, T., Asakawa, S., Hattori, N., Matsumine, H., Yamamura, Y., Minoshima, S., Yokochi, M., Mizuno, Y., and Shimizu, N. (1998). Mutations in the parkin gene cause autosomal recessive juvenile parkinsonism. Nature *392*, 605–608.

Kitada, T., Pisani, A., Porter, D.R., Yamaguchi, H., Tscherter, A., Martella, G., Bonsi, P., Zhang, C., Pothos, E.N., and Shen, J. (2007). Impaired dopamine release and synaptic plasticity in the striatum of PINK1-deficient mice. Proc. Natl. Acad. Sci. USA *104*, 11441–11446.

Klionsky, D.J., Abdelmohsen, K., Abe, A., Abedin, M.J., Abeliovich, H., Acevedo Arozena, A., Adachi, H., Adams, C.M., Adams, P.D., Adeli, K., et al. (2016). Guidelines for the use and interpretation of assays for monitoring autophagy (3rd edition). Autophagy *12*, 1–222.

Kuiper, R.P., Schepens, M., Thijssen, J., van Asseldonk, M., van den Berg, E., Bridge, J., Schuuring, E., Schoenmakers, E.F., and van Kessel, A.G. (2003). Upregulation of the transcription factor TFEB in t(6;11)(p21;q13)-positive renal cell carcinomas due to promoter substitution. Hum. Mol. Genet. *12*, 1661–1669.

Lin, M.T., and Beal, M.F. (2006). Mitochondrial dysfunction and oxidative stress in neurodegenerative diseases. Nature *443*, 787–795.

Liu, S., and Lu, B. (2010). Reduction of protein translation and activation of autophagy protect against PINK1 pathogenesis in *Drosophila melanogaster*. PLoS Genet. *6*, e1001237.

MacRae, C.A., and Peterson, R.T. (2015). Zebrafish as tools for drug discovery. Nat. Rev. Drug Discov. *14*, 721–731.

Morais, V.A., Verstreken, P., Roethig, A., Smet, J., Snellinx, A., Vanbrabant, M., Haddad, D., Frezza, C., Mandemakers, W., Vogt-Weisenhorn, D., et al. (2009). Parkinson's disease mutations in PINK1 result in decreased Complex I activity and deficient synaptic function. EMBO Mol. Med. *1*, 99–111.

Murtaza, M., Shan, J., Matigian, N., Todorovic, M., Cook, A.L., Ravishankar, S., Dong, L.F., Neuzil, J., Silburn, P., Mackay-Sim, A., et al. (2016). Rotenone susceptibility phenotype in olfactory derived patient cells as a model of idiopathic Parkinson's disease. PLoS One *11*, e0154544.

Nezich, C.L., Wang, C., Fogel, A.I., and Youle, R.J. (2015). MiT/TFE transcription factors are activated during mitophagy downstream of Parkin and Atg5. J. Cell Biol. *210*, 435–450.

Pankiv, S., Clausen, T.H., Lamark, T., Brech, A., Bruun, J.A., Outzen, H., Overvatn, A., Bjorkoy, G., and Johansen, T. (2007). p62/SQSTM1 binds directly to Atg8/LC3 to facilitate degradation of ubiquitinated protein aggregates by autophagy. J. Biol. Chem. *282*, 24131–24145.

Parganlija, D., Klinkenberg, M., Dominguez-Bautista, J., Hetzel, M., Gispert, S., Chimi, M.A., Drose, S., Mai, S., Brandt, U., Auburger, G., et al. (2014). Loss of PINK1 impairs stress-induced autophagy and cell survival. PLoS One *9*, e95288.

Park, J., Lee, S.B., Lee, S., Kim, Y., Song, S., Kim, S., Bae, E., Kim, J., Shong, M., Kim, J.M., et al. (2006). Mitochondrial dysfunction in *Drosophila* PINK1 mutants is complemented by parkin. Nature *441*, 1157–1161.

Parker, W.D., Jr., and Swerdlow, R.H. (1998). Mitochondrial dysfunction in idiopathic Parkinson disease. Am. J. Hum. Genet. *62*, 758–762.

Pickrell, A.M., and Youle, R.J. (2015). The roles of PINK1, parkin, and mitochondrial fidelity in Parkinson's disease. Neuron *85*, 257–273.

Rink, E., and Wullimann, M.F. (2001). The teleostean (zebrafish) dopaminergic system ascending to the subpallium (striatum) is located in the basal diencephalon (posterior tuberculum). Brain Res. *889*, 316–330.

Roczniak-Ferguson, A., Petit, C.S., Froehlich, F., Qian, S., Ky, J., Angarola, B., Walther, T.C., and Ferguson, S.M. (2012). The transcription factor TFEB links mTORC1 signaling to transcriptional control of lysosome homeostasis. Sci. Signal *5*, ra42.

Sallinen, V., Torkko, V., Sundvik, M., Reenila, I., Khrustalyov, D., Kaslin, J., and Panula, P. (2009). MPTP and MPP^+ target specific aminergic cell populations in larval zebrafish. J. Neurochem. *108*, 719–731.

Sardiello, M., Palmieri, M., di Ronza, A., Medina, D.L., Valenza, M., Gennarino, V.A., Di Malta, C., Donaudy, F., Embrione, V., Polishchuk, R.S., et al. (2009). A gene network regulating lysosomal biogenesis and function. Science *325*, 473–477.

Schapira, A.H., Olanow, C.W., Greenamyre, J.T., and Bezard, E. (2014). Slowing of neurodegeneration in Parkinson's disease and Huntington's disease: future therapeutic perspectives. Lancet *384*, 545–555.

Settembre, C., Di Malta, C., Polito, V.A., Garcia Arencibia, M., Vetrini, F., Erdin, S., Erdin, S.U., Huynh, T., Medina, D., Colella, P., et al. (2011). TFEB links autophagy to lysosomal biogenesis. Science *332*, 1429–1433.

Settembre, C., Zoncu, R., Medina, D.L., Vetrini, F., Erdin, S., Erdin, S., Huynh, T., Ferron, M., Karsenty, G., Vellard, M.C., et al. (2012). A lysosome-to-nucleus signalling mechanism senses and regulates the lysosome via mTOR and TFEB. EMBO J. *31*, 1095–1108.

Song, S., Jang, S., Park, J., Bang, S., Choi, S., Kwon, K.Y., Zhuang, X., Kim, E., and Chung, J. (2013). Characterization of PINK1 (PTEN-induced putative kinase 1) mutations associated with Parkinson disease in mammalian cells and *Drosophila*. J. Biol. Chem. *288*, 5660–5672.

Song, W., Wang, F., Lotfi, P., Sardiello, M., and Segatori, L. (2014). 2-Hydroxypropyl-beta-cyclodextrin promotes transcription factor EB-mediated activation of autophagy: implications for therapy. J. Biol. Chem. *289*, 10211–10222.

Tanner, C.M., Kamel, F., Ross, G.W., Hoppin, J.A., Goldman, S.M., Korell, M., Marras, C., Bhudhikanok, G.S., Kasten, M., Chade, A.R., et al. (2011). Rotenone, paraquat, and Parkinson's disease. Environ. Health Perspect. *119*, 866–872.

Trinh, J., and Farrer, M. (2013). Advances in the genetics of Parkinson disease. Nat. Rev. Neurol. *9*, 445–454.

Tsvetkov, A.S., Miller, J., Arrasate, M., Wong, J.S., Pleiss, M.A., and Finkbeiner, S. (2010). A small-molecule scaffold induces autophagy in primary neurons and protects against toxicity in a Huntington disease model. Proc. Natl. Acad. Sci. USA *107*, 16982–16987.

Valente, E.M., Abou-Sleiman, P.M., Caputo, V., Muqit, M.M., Harvey, K., Gispert, S., Ali, Z., Del Turco, D., Bentivoglio, A.R., Healy, D.G., et al. (2004). Hereditary early-onset Parkinson's disease caused by mutations in PINK1. Science *304*, 1158–1160.

Vandonselaar, M., Hickie, R.A., Quail, J.W., and Delbaere, L.T. (1994). Trifluoperazine-induced conformational change in Ca(2+)-calmodulin. Nat. Struct. Biol. *1*, 795–801.

Varga, M., Sass, M., Papp, D., Takacs-Vellai, K., Kobolak, J., Dinnyes, A., Klionsky, D.J., and Vellai, T. (2014). Autophagy is required for zebrafish caudal fin regeneration. Cell Death Differ. *21*, 547–556.

Vilain, S., Esposito, G., Haddad, D., Schaap, O., Dobreva, M.P., Vos, M., Van Meensel, S., Morais, V.A., De Strooper, B., and Verstreken, P. (2012). The yeast complex I equivalent NADH dehydrogenase rescues pink1 mutants. PLoS Genet. *8*, e1002456.

Wood-Kaczmar, A., Gandhi, S., Yao, Z., Abramov, A.Y., Miljan, E.A., Keen, G., Stanyer, L., Hargreaves, I., Klupsch, K., Deas, E., et al. (2008). PINK1 is necessary for long term survival and mitochondrial function in human dopaminergic neurons. PLoS One *3*, e2455.

Yang, Y., Gehrke, S., Imai, Y., Huang, Z., Ouyang, Y., Wang, J.W., Yang, L., Beal, M.F., Vogel, H., and Lu, B. (2006). Mitochondrial pathology and muscle and dopaminergic neuron degeneration caused by inactivation of *Drosophila* Pink1 is rescued by Parkin. Proc. Natl. Acad. Sci. USA *103*, 10793–10798.

Yue, Z., Friedman, L., Komatsu, M., and Tanaka, K. (2009). The cellular pathways of neuronal autophagy and their implication in neurodegenerative diseases. Biochim. Biophys. Acta *1793*, 1496–1507.

Please cite this article in press as: Zhang et al., Rescue of Pink1 Deficiency by Stress-Dependent Activation of Autophagy, Cell Chemical Biology (2017), http://dx.doi.org/10.1016/j.chembiol.2017.03.005

STAR★METHODS

KEY RESOURCES TABLE

REAGENT or RESOURCE	SOURCE	IDENTIFIER
Antibodies		
Mouse monoclonal anti-Tyrosine Hydroxylase	Novus Biologicals	clone 2D3.1G7
Mouse monoclonal anti-MTCO2	Abcam	clone 12C4F12
Rabbit monoclonal anti-Pink1	Cell Signaling	RRID: AB_11179069
Mouse monoclonal anti-SQSTM1	Abnova	RRID: AB_437085
Rabbit polyclonal anti-LC3	Novus Biologicals	RRID: AB_578334
Rabbit anti-β-actin	Abcam	RRID: AB_230518
Alexa-488 anti-mouse	Jackson Immuno Research Laboratories, INC.	715-546-150
Alexa-647 anti-rabbit	Jackson Immuno Research Laboratories, INC.	711-606-152
Chemicals, Peptides, and Recombinant Proteins		
Rotenone	Sigma-Aldrich	R8875
Antimycin A	Sigma-Aldrich	A8674
Pericidin A	Cayman Chemical	15379
Bafilomycin A1	Sigma-Aldrich	B1793
NIH Clinical Collection	Evotec	NIHCC1/NIHCC2
2,6-Dichloroindophenol sodium salt hydrate (DCIP)	Sigma-Aldrich	D1878
Decylubiquinone	Sigma-Aldrich	D7911
NADH	Sigma-Aldrich	N8129
JC-1 dye	Sigma-Aldrich	CS0390
FCCP	Sigma-Aldrich	C2920
Oligomycin	Selleckchem	S1478
DMSO	Thermo Fisher	AJA2225-500ML
Pronase	Sigma-Aldrich	10165921001
Trifluoperazine	Sigma-Aldrich	T8516
Prochlorperazine	Sigma-Aldrich	P9178
Fluphenazine	Sigma-Aldrich	F4765
Quinolyl-valyl-O-methylaspartyl-[-2,-difluorophenoxy]-methyl ketone (QVD)	Abcam	Ab141421
Triton X-100	Sigma-Aldrich	93443
Bovine Serum Albumin	Sigma-Aldrich	A9418
ProLong Diamond Antifade Reagent	Thermo Fisher	P36934
Paraformaldehyde	Proscitech	C004
DAPI	Sigma-Aldrich	D9542
Tween-20	Sigma-Aldrich	P9416
Rapamycin	Sigma-Aldrich	R0395
(2-Hydroxypropyl)-β-cyclodextrin	Sigma-Aldrich	H107
10-NCP	Merck Millipore	124020
Puromycin	Selleckchem	S7417
Penicillin-streptomycin 100x stock	Thermo Fisher	15140122
Protease inhibitor cocktail	Roche	4693159001
Phosphatase inhibitor	Cell signaling	5870
Commercial Assays		
Mitochondria Isolation Kit	Sigma-Aldrich	MITOISO1
ATP Bioluminescence Assay Kit CLS II	Roche Life Sciences	1699695

(*Continued on next page*)

Continued

REAGENT or RESOURCE	SOURCE	IDENTIFIER
MitoSOX Red	Thermo fisher	M36008
SYBR FAST One-Step qPCR Kit	KAPA Biosystems	KK4651
Direct-zol RNA MiniPrep Kit	Zymo Research	R2050
Pierce™ BCA Protein Assay Kit	Thermo Fisher	23225
Experimental Models: Cell Lines		
HEK293T	ATCC	RRID: CVCL_0063
SH-SY5Y	ATCC	RRID: CVCL_0019
Experimental Models: Organisms/Strains		
Zebrafish *pink1*^{gi2}	This paper	
Oligonucleotides		
5'-GGCAATGAAGATGATGTGGAAC 5'-TCTTAAAGCTTGTGGGCATGAA	IDT	Zebrafish pink1
5'-GCGCCCTTCCAAATGTACTA 5'-CCAGGAATTCCATGAGGAGA	IDT	Zebrafish p62
5'-TGAAGACAGCAGAAGTCAATG 5'-CAGTAAACATGTCAGGCTAAATAA	IDT	Zebrafish hatn10
5'-CAGAGAAGCCCATGGACAG 5'-AGCTGCCTTGTACCCACATC	IDT	Human P62
5'-CCAGAAGCGAGAGCTCACAGAT 5'-TGTGATTGTCTTTCTTCTGCCG	IDT	Human TFEB
5'-ACGTTACAGCGTCCAGCTCAT 5'-TCTTTGGAGCTCGCATTGG	IDT	Human LAMP1
5'-GGAAGTGTCAGATGATCCCCA 5'-CCGTTTGCCTCGTGGATAAT	IDT	Human ATP6V1H
5'-TGCACCACCAACTGCT 5'-GGCATGGACTGTGGTCATGAG	IDT	Human GAPDH
5'-CCTTGTCATCTGCCATTATCATCGT	Gene Tools	ATG5 Morpholino
Recombinant DNA		
shControl	Sigma-Aldrich	#SHC002
shPINK1	Sigma-Aldrich	#SHCLND-NM_032409
pEGFP-N1-TFEB	Addgene	38119
YFP-Parkin	Addgene	23955
Software and Algorithms		
GraphPad Prism	GraphPad Software Inc	http://www.graphpad.com/scientific-software/prism/
Image J	ImageJ	https://imagej.nih.gov/ij/

CONTACT FOR REAGENT AND RESOURCE SHARING

Further information and requests for resources and reagents should be directed to the Lead Contact, Daniel Hesselson (d.hesselson@garvan.org.au).

EXPERIMENTAL MODEL AND SUBJECT DETAILS

Zebrafish

Fertilized eggs were collected from zebrafish (*Danio rerio*) group matings. Embryos were incubated at 28.5 °C. At 1 dpf, the chorion was removed by digestion with Pronase (10 μg/mL; Sigma-Aldrich) overnight. Drug treatments were performed in embryo media (0.6 g/L ocean salt supplemented with 1.5 g/L CaCl) buffered with 10 mM HEPES (ThermoFisher). Both sexes were used; zebrafish sex is indeterminable at this stage. The Garvan Institute of Medical Research Animal Ethics Committee approved all zebrafish protocols.

Cell Lines

SH-SY5Y cells were cultured in DMEM/F12 (GIBCO) supplemented with 10% fetal bovine serum (FBS), penicillin (100 U/mL) and streptomycin (100 μg/mL). HEK293T cells were cultured in DMEM (GIBCO) supplemented with 10% fetal bovine serum (FBS), penicillin (100 U/mL) and streptomycin (100 μg/mL). Both cell lines were grown at 37 °C in a humidified 5% CO_2 incubator. All experiments were performed with cell cultures that had been passaged less than 8 times since receipt from ATCC.

METHODS DETAIL

TALEN Mutagenesis

A pair of TALENs targeting zebrafish *pink1* exon 6 were constructed by the 'golden gate' method (Cermak et al., 2011). TALEN mRNA was synthesised by in vitro transcription using the SP6 mMESSAGE mMACHINE Kit (Ambion). 100 pg of mRNA encoding each TALEN heterodimer was injected into the cytoplasm of the cell of one cell-stage wild-type zebrafish embryos. The *pink1*^{gi2} strain harbours a 10 bp deletion (ΔTTCAGCAGCT) in exon 6 resulting in a frameshift and a premature stop codon after amino acid 387.

Touch-Evoked Escape Response

Two zebrafish (2 dpf) per well were plated in 96-well glass plates (Zinsser) for behavioral assays (200 μL per well). At this density individual animals could be manually manipulated with a probe. Rotenone, antimycin A or piericidin A (Sigma-Aldrich) were added to a final concentration of 0.1-10,000 nM, covered with oxygen permeable seals (Sigma-Aldrich) and incubated for 24 h in humidified chambers at 28.5 °C. Individual wells were observed at 50x magnification and each zebrafish was lightly probed near the tip of the tail to stimulate the escape response. Each well was scored; 0, no movement. 1, one zebrafish responded. 2, both zebrafish responded. For Atg5 knockdown experiments, 2 ng control or *atg5* morpholino (Varga et al., 2014) was injected at the 1-cell stage.

Chemical Screen

Zebrafish *pink1*(-/-) mutants (50 hpf) were pretreated with the NIH Clinical Collection (Evotec; 1 mM in DMSO) at a 1:100 final dilution in HEPES (10 mM) buffered embryo medium. Stock solutions (1 mM) were added directly to the wells of a 96-well plate and incubated for 2 h at 28.5 °C. Retests and subsequent assays were also performed using 1:100 final dilutions of drugs purchased from Sigma-Aldrich. All compounds were dissolved in DMSO (1% final concentration). Rotenone stock solution (1 mM in EtOH) was diluted to 4.5 μM with 5 mM potassium phosphate buffer (pH 7.4) and added at a 1:100 dilution to a final concentration of 45 nM (0.0045% final EtOH concentration). The plates were incubated from 52 to 76 hpf at 28.5 °C and scored in the TEER assay. Each plate contained wild-type and *pink1*(-/-) DMSO treated controls. Data from the entire plate were excluded if the wild-type controls failed to respond or the *pink1*(-/-) controls exhibited a response.

Mitochondrial Isolation

Mitochondria were isolated using the Mitochondrial Isolation Kit (Sigma-Aldrich) according to the manufacturer's protocol. Briefly, zebrafish embryos were washed twice with Extraction Buffer A (EBA) and homogenized in 10 volumes of EBA containing 2 mg/mL albumin. Samples were centrifuged at 600 x *g* for 5 minutes to remove debris and the supernatant was transferred to new tubes and centrifuged at 11,000 x *g* for 10 minutes to pellet mitochondria. The mitochondria were washed in 10 volumes of EBA, collected by centrifugation at 11,000 x *g* for 10 minutes and resuspended in Storage Buffer.

Complex I Activity

The complex I activity of isolated mitochondria was measured as described (Janssen et al., 2007). Briefly, 5 μg of isolated mitochondria (in 40 μL) was incubated with 960 μL reaction mixture (25 mM potassium phosphate, 3.5 g/L BSA, 60 μM DCIP, 70 μM decylubiquinone, 1 μM antimycin A, pH 7.8). After 3 minutes 20 μL NADH (10 mM) was added and the absorbance (600 nm) was measured at 30 second intervals for 4 minutes at 37°C. One μL rotenone (1 mM) was added to terminate the reaction and determine the background activity. For acute treatments, 5 μg of isolated mitochondria were incubated with rotenone (80 nM) and/or TFP (5 μM) for 2 min immediately before determination of complex I activity.

Mitochondrial Membrane Potential

Mitochondrial membrane potential of isolated mitochondria was measured using the JC-1 dye (Sigma-Aldrich) according to the manufacturer's protocol. 5 μg of protein was used for each reaction. Wild-type mitochondria were treated with 2 μM FCCP or 2 μM oligomycin to establish the dynamic range of the JC-1 dye.

ATP Content

The ATP content of isolated mitochondria and homogenized zebrafish was measured using the ATP Bioluminescence Assay Kit CLS II (Roche Life Science) according to the manufacturer's protocol.

ROS Production

The ROS levels in isolated mitochondria were measured using MitoSOX Red (Thermofisher Scientific). MitoSOX Red (5 μM) was added to 5 μg of isolated mitochondria and incubated for 10 min at 37 °C. Fluorescence was measured with a CLARIOstar (BMG Labtech) microplate reader (510 nm excitation/ 595 nm emission).

Mitochondrial Stress Test

The in vivo oxygen consumption rate was determined using an XF24 analyzer (Seahorse Biosciences) as described (Gibert et al., 2013). Zebrafish were dispensed into XF24 islet capture plates. Hydration of the sensor cartridge was carried out at 28.5 °C and all measurements were taken at 28.5 °C. Eight cycles (2 minutes mix, 1 minute incubation, 2 minutes data acquisition) were acquired between each injection. All compounds were dissolved in DMSO at 2.5 mM and diluted in embryo media to the final concentration (25 μM oligomycin, 2.5 μM FCCP, 25 μM rotenone and 25 μM antimycin A).

Tissue Culture and Drug Treatments

EGFP-TFEB (Addgene #38119) and YFP-PARKIN (Addgene #23955) plasmids were transfected using ViaFect Transfection Reagent (Promega). Trifluoperazine, prochlorperazine, fluphenazine, 10-NCP, and rapamycin (Sigma-Aldrich) were used at 10 μM (6 h treatments) or 8 μM (24 h treatments). (2-Hydroxypropyl)-β-cyclodextrin (Sigma-Aldrich) was used at 1 mM. 10 μg/mL oligomycin and 5 μg/mL antimycin A were used for 6 h treatments. 5 μg/mL oligomycin and 2.5 μg/mL antimycin A were used for 24 h treatments. 10 μM quinolyl-valyl-O-methylaspartyl-[-2,-difluorophenoxy]-methyl ketone (QVD) was used to prevent apoptosis during 24 h assays. Lysosomal function was blocked with 1 h bafilomycin A1 (100 nM) treatment.

Lentiviral PINK1 Knockdown

shControl (#SHC002) and shPINK1 (#SHCLND-NM_032409) plasmids from Sigma-Aldrich were transfected into HEK293T cells together with Gag-Pol and VSV-G lentiviral packaging plasmids using ViaFect transfection reagent (Promega). Viral supernatant was harvested after 48 h and used to infect SH-SY5Y cells. Experiments were performed after 72 h puromycin (2 μg/mL) selection.

Quantitative Real-Time PCR

RNA was isolated from zebrafish and SH-SY5Y cells using the Direct-zol RNA MiniPrep Kit (Zymo Research). Real-time PCR was performed using the SYBR FAST One-Step qPCR Kit (KAPA Biosystems). Samples were reverse transcribed at 42 °C for 5 minutes, inactivated at 95 °C for 3 minutes and PCR amplified (40 cycles of 95 °C for 10 s, 60 °C for 30 s, and 72 °C for 30 s). Gene expression was normalized to *hatn10* (zebrafish) or *GAPDH* (human) and fold change was calculated using the ΔΔCt method (see primer sequences in Key Resources Table).

Immunostaining and Confocal Microscopy

Zebrafish were fixed in 8% paraformaldehyde overnight at 4 °C. Brain tissue was manually dissected and blocked for 1 h in PBS with 0.1% Triton X-100, 1% BSA and 5% serum. Primary and secondary antibodies (in PBS with 0.1% Triton X-100, 1% BSA and 1% serum) were incubated overnight at 4 °C and samples were mounted in ProLong Diamond Antifade Reagent (Thermo Fisher). SH-SY5Y cells were fixed with 4% paraformaldehyde for 15 min and blocked in PBS with 0.1% Triton X-100 and 3% serum for 1 h. Cells were incubated with primary antibody overnight at 4 °C followed by secondary antibody (1 h) and 4',6-diamidino-2-phenylindole (DAPI) staining (10 minutes) at room temperature. All images were acquired with a Leica DMI 6000 SP8 confocal microscope. Z-stacks of TH-stained neurons were quantified using ImageJ to uniquely mark individual cells. Cytoplasmic EGFP-TFEB localization was quantified by subtracting the nuclear EGFP signal (defined by DAPI staining) from the total EGFP signal from individual cells using ImageJ. Thresholded Pearson correlations for MTCO2/YFP-PARKIN co-localization were determined using the Costes thresholding method with 100 iterations implemented in the Coloc2 module (ImageJ).

Western Blotting

Zebrafish were deyolked by passing through a 200 μL pipette tip and rinsed twice with ice cold Ringer's solution. Deyolked zebrafish and SH-SY5Y cells were lysed in RIPA buffer containing protease inhibitor cocktail (Roche) and phosphatase inhibitor (Cell Signaling Technology). Protein concentrations were measured by BCA (Thermo Scientific). Equal amounts of protein were separated on 10% or 12% SDS-PAGE gels (Bio-Rad) and transferred to PVDF membranes that were blocked with TBS containing 0.1% Tween-20 and 5% BSA. Membranes were incubated with primary antibodies overnight at 4 °C followed by secondary antibodies at room temperature for 1 h and were developed with Clarity Western ECL (Bio-Rad) and imaged for densitometry (Fusion FX7, Vilber).

QUANTIFICATION AND STATISTICAL ANALYSIS

All data fitting and statistical analysis performed using Graphpad Prism version 7.0a for Mac OS X, Graphpad Software, www.graphpad.com. Statistical values including the exact *n* and statistical significance are reported in the Figures and/or Figure Legends. Statistical tests and analysis methods are described in the Figure Legends. Statistical significance was defined as $p < 0.05$.